*Inorg. Chem.* **2005**, *44*, 9143–9153


# Crystal Structures and Magnetic Properties of Mixed Iridium–Ruthenium Triple Perovskites. 1. $Ba_3MRuIrO_9$ (M = Lanthanide, Y)

**Michael W. Lufaso and Hans-Conrad zur Loye***

*Department of Chemistry and Biochemistry, University of South Carolina, Columbia, South Carolina 29208*

Received August 5, 2005

Crystal structures and magnetic properties of $Ba_3MRuIrO_9$ (M = lanthanides, Y) were investigated. Rietveld refinements using powder diffraction data indicate that all the compounds crystallize in the 6H-$BaTiO_3$ structure type in space group $P6_3/mmc$. Magnetic susceptibility measurements were carried out on each compound. Effective magnetic moments were smaller than values estimated using spin-only moments, which indicate the presence of spin–orbit coupling and strong interactions in the $[(Ru_{0.5}Ir_{0.5})_2O_9]$ face-sharing octahedra that contain a disordered mixture of Ru and Ir on a single crystallographic site. Magnetic anomalies were observed for the compounds $Ba_3PrRuIrO_9$, $Ba_3TbRuIrO_9$, and $Ba_3NdRuIrO_9$ at 3.5, 13, and 8 K, respectively.

## 1. Introduction

The perovskite oxide, $AMO_3$, family of compounds is perhaps the most widely studied in the field of solid-state chemistry.[1] The compositional flexibility of the perovskite structure type enables nearly every element in the periodic table to be incorporated into the structure, which leads to diverse and interesting physical properties. Many studies have focused on specific physical properties, such as complex magnetic phenomena, superconductivity, ferroelectricity, piezoelectricity, and diverse transport properties, all of which rely on a solid understanding of the structural variations within this family. The ideal cubic $AMO_3$ perovskite may be described as having corner-sharing $MO_6$ octahedra, with the A-site cation occupying the 12-coordinate site in the center of the cube formed by the $MO_3$ network. The 2H hexagonal perovskite consists of infinite chains of face-sharing octahedra that are separated by chains of A-site cations.[2] Alternatively, perovskites and related structures may also be thought of as resulting from the stacking of close-packed $AO_3$ layers and the filling of the resultant octahedral sites by the M cation. An ABC stacking of the $AO_3$ layers results in the cubic perovskite, while an AB stacking results in the 2H perovskite structure. Intergrowth structures, including the $A_3MM_2'O_9$ triple perovskites of this study, contain both corner-sharing and face-sharing octahedra, consistent with ABC and AB stacking, respectively.

The quaternary triple perovskite oxides, $Ba_3MRu_2O_9$ and $Ba_3MIr_2O_9$ (M = alkali, alkaline earth, transition metal, and lanthanide cations), have been the subject of numerous investigations focusing on their structures and magnetic properties.[3−12] Most of these compounds adopt the 6H-$BaTiO_3$ structure type, crystallizing in space group $P6_3/mmc$, in which the smaller metal cations (e.g., Ir or Ru) occupy the face-sharing octahedral site while the larger M cation occupies the corner-sharing octahedral site. A few compounds adopt closely related crystal structures that have the same polyhedral connectivity as the 6H-$BaTiO_3$-type structure, including $Ba_3BiRu_2O_9$, $Ba_3LaIr_2O_9$, and $Ba_3NdIr_2O_9$ compounds; however, they crystallize in space group $C2/c$.[7,11] Other compounds exist in the 6H-$BaTiO_3$ structure at room temperature but undergo a structure change as a function of

* Author to whom correspondence should be addressed. Tel.: (803) 777-6916. Fax: (803) 777-8508. E-mail: zurloye@mail.chem.sc.edu.

(1) Mitchell, R. H. *Perovskites: Modern and Ancient*; Almaz Press: Ontario, Canada, 2002.
(2) Stitzer, K. E.; Darriet, J.; zur Loye, H.-C. *Curr. Opin. Solid State Mater. Sci.* **2001**, *5*, 535.
(3) Doi, Y.; Wakeshima, M.; Hinatsu, Y.; Tobo, A.; Ohoyama, K.; Yamaguchi, Y. *J. Mater. Chem.* **2001**, *11*, 3135.
(4) Doi, Y.; Hinatsu, Y.; Shimojo, Y.; Ishii, Y. *J. Solid State Chem.* **2001**, *161*, 113.
(5) Doi, Y.; Hinatsu, Y. *J. Solid State Chem.* **2004**, *177*, 3239.
(6) Hinatsu, Y.; Oyama, S.; Doi, Y. *Bull. Chem. Soc. Jpn.* **2004**, *77*, 1479.
(7) Doi, Y.; Hinatsu, Y. *J. Phys.: Condens. Matter.* **2004**, *16*, 2849.
(8) Doi, Y.; Matsuhira, K.; Hinatsu, Y. *J. Solid State Chem.* **2002**, *165*, 317.
(9) Doi, Y.; Wakeshima, M.; Hinatsu, Y.; Tobo, A.; Ohoyama, K.; Yamaguchi, Y. *J. Alloys Compd.* **2002**, *344*, 166.
(10) Gonen, Z. S.; Gopalakrishnan, J.; Eichhorn, B. W.; Greene, R. L. *Inorg. Chem.* **2001**, *40*, 4996.
(11) Darriet, J.; Bontchev, R.; Dussarrat, C.; Weill, F.; Darriet, B. *Eur. J. Solid State Inorg. Chem.* **1993**, *30*, 273.
(12) Thumm, I.; Treiber, U.; Kemmler-Sack, S. *J. Solid State Chem.* **1980**, *35*, 156.

10.1021/ic051344z CCC: $30.25 
Published on Web 11/12/2005

temperature. For example, upon cooling, $Ba_3NdRu_2O_9$ undergoes a magnetic transition and a concomitant structural phase transition to $C2/c$,[4] while $Ba_3NaRu_2O_9$ undergoes[13] charge ordering of $Ru^{5+}$ and $Ru^{6+}$ accompanied by a phase transition from space group $P6_3/mmc$ to $Cmcm$. $Ba_3CuRu_2O_9$, meanwhile, crystallizes in space group $Cmcm$ at ambient temperatures,[14] whereas $Ba_3CoRu_2O_9$ undergoes a phase transition from $P6_3/mmc$ at room temperature to space group $Cmcm$ at 2 K.[15] Similarly, $Ba_3NaIr_2O_9$ undergoes a phase transition from $P6_3/mmc$ at room temperature to space group $C2/c$ near 190 K.[16]

Magnetic properties in the series of triple perovskites $Ba_3MRu_2O_9$ and $Ba_3MIr_2O_9$ are primarily the result of the interactions between the Ru ions in the $[Ru_2O_9]$ dimer or the Ir ions in the $[Ir_2O_9]$ dimer and the interaction between the M and Ru or M and Ir ions along the linear M−O−Ru or M−O−Ir pathway.[17] It is worth noting that, in the 6H-$BaTiO_3$ and related structures, the short Ru−Ru and Ir−Ir bond distances (2.5−2.75 Å) in the face-sharing dimer promote strong orbital interactions between the magnetic cations. In general, the magnetic susceptibilities show a broad maximum in the 125−400 K temperature range, large spin−orbit coupling, and in some cases a magnetic transition between 4 and 24 K.[3,5−9,17−20] In mixed iridium−ruthenium triple perovskites $Ba_3MRu_{2-x}Ir_xO_9$ ($0 < x < 2$), the literature contains crystal structure information on only $Ba_3SmRuIrO_9$ and $Ba_3CaRu_{0.5}Ir_{1.5}O_9$.[21,22] $Ba_3M^{3+}RuIrO_9$ were briefly investigated, but detailed information concerning their crystal structures and magnetic properties were not reported.[23] In the $Ba_3MRu_{2-x}Ir_xO_9$ series, the $x = 1$ members are of particular interest because these compounds are the most likely to exhibit charge or chemical ordering or would show the greatest influence of disorder on the properties. In this paper, we report on the crystal chemistry and magnetic properties of the mixed ruthenium−iridium triple-perovskite series $Ba_3MRuIrO_9$ (M = Y, lanthanides).

## 2. Experimental Section

Black polycrystalline samples were prepared by conventional solid-state methods. $RuO_2$ was prepared from Ru metal (Engelhard, 99.5%) by heating it in air to 950 °C for 48 h with an intermediate grinding. The starting reactant materials were $RuO_2$, Ir (Engelhard, 99.5%), $BaCO_3$ (Alfa Aesar, 99.95%), and high-purity lanthanide oxides. The lanthanide oxides were dried overnight and stored in a desiccator prior to use. The starting materials were weighed in the correct ratios and mixed in an agate mortar with acetone. The samples were calcined overnight in high-form alumina crucibles. The synthesis temperature ranged from 1100 to 1225 °C with intermediate grinding. The final annealing conditions for all compounds can be found in the Supporting Information. Heating cycles of the samples were continued for between 2 and 10 days until changes in the weakest peaks were no longer evident.

X-ray powder diffraction data were collected using a Rigaku DMAX 2200 diffractometer. Data were collected at 0.03° steps for 12.5 s/step over the $2\theta$ range 5−110°. Rietveld refinements were performed using the EXPGUI GSAS package.[24,25] Magnetic susceptibility measurements were made using a Quantum Design MPMS XL SQUID magnetometer. The powder samples were placed inside a gelatin capsule and inserted into a plastic straw. The small diamagnetic contribution of the gelatin capsule had a negligible contribution to the overall magnetization, which was dominated by the sample. Data were collected after cooling in the absence of an applied field [zero-field cooled (ZFC)] and after cooling in a magnetic field [field-cooled (FC)] of 1 kG. Measurements for determining the field dependence of the magnetic susceptibility were performed in applied fields between 0 and 40 kG for $Ba_3NdRuIrO_9$.

## 3. Results and Discussion

**3.a. Crystal Structures.** The series $Ba_3MRuIrO_9$ (M = Y, lanthanides) was synthesized as polycrystalline powders by solid-state methods and structurally investigated by powder X-ray diffraction. Systematic absences in the intensity data for all compositions were consistent with the space group $P6_3/mmc$. This is not unexpected as the majority of $Ba_3MIr_2O_9$ and $Ba_3MRu_2O_9$ compounds are known to crystallize in space group $P6_3/mmc$.[7,8,13,26] Only one $x = 1$ mixed iridium−ruthenium triple-perovskite crystal structure has been reported, $Ba_3SmRuIrO_9$; however, its atomic positions in space group $P6_3/mmc$ were not refined.[21] The iridates $Ba_3LnIr_2O_9$ (Ln = La, Nd) [7] were reported to crystallize in space group $C2/c$, whereas the analogous ruthenates $Ba_3LnRu_2O_9$ (Ln = La, Nd)[4,7] crystallize in space group $P6_3/mmc$. In this study, the mixed Ir/Ru compositions $Ba_3LnRuIrO_9$ (Ln = La, Nd) were both found to crystallize in space group $P6_3/mmc$.

X-ray diffraction profiles for $Ba_3LaRuIrO_9$ and $Ba_3LuRuIrO_9$ are shown in Figure 1. The inset shows the separation of the strongest reflections, 104 and 110. The separation between the peaks is larger for $Ba_3LaRuIrO_9$ compared to $Ba_3LuRuIrO_9$ because the crystal structure accommodates the larger M cation (La vs Lu) primarily by expansion along the $c$ axis, thus, shifting the 104 reflection disproportionally to lower angles compared to the 110 reflection. The crystal structure of $Ba_3LaRuIrO_9$ is shown in Figure 2. $Ba_3LaRuIrO_9$ has a corner-sharing octahedral site occupied by La and a face-sharing octahedral site occupied by a disordered mixture of Ru and Ir. Refinements attempted in space group $P6_3/mc$, which allows for an ordered arrangement of Ru and Ir in the face-sharing dimer,


(13) Stitzer, K. E.; Smith, M. D.; Gemmill, W. R.; zur Loye, H.-C. *J. Am. Chem. Soc.* **2002**, *124*, 13877.
(14) Rijssenbeek, J. T.; Huang, Q.; Erwin, R. W.; Zandbergen, H. W.; Cava, R. J. *J. Solid State Chem.* **1999**, *146*, 65.
(15) Lightfoot, P.; Battle, P. D. *J. Solid State Chem.* **1990**, *89*, 174.
(16) Macquart, R.; zur Loye, H.-C. *J. Solid State Chem.* **2005**, submitted.
(17) Darriet, J.; Dillon, M.; Villeneuve, G.; Hagenmuller, P. *J. Solid State Chem.* **1976**, *19*, 213.
(18) Doi, Y.; Hinatsu, Y. *J. Mater. Chem.* **2002**, *12*, 1792.
(19) Oyama, S.; Doi, Y.; Hinatsu, Y.; Ishii, Y. *Bull. Chem. Soc. Jpn.* **2004**, *77*, 1359.
(20) Byrne, R. C.; Moeller, C. W. *J. Solid State Chem.* **1970**, *2*, 228.
(21) Thumm, I.; Treiber, U.; Kemmler-Sack, S. *Z. Anorg. Allg. Chem.* **1981**, *477*, 161.
(22) Scheske, S.; Müller-Buschbaum, H. *J. Alloys Compd.* **1993**, *198*, 173.
(23) Duerrschmidt, E.; Kemmler-Sack, S. *Z. Anorg. Allg. Chem.* **1980**, *470*, 109.
(24) Larson, A. C.; von Dreele, R. B. *General Structure Analysis System (GSAS)*; Los Alamos National Laboratories: Los Alamos, NM, 1990.
(25) Toby, B. H. *J. Appl. Crystallogr.* **2001**, *34*, 210.
(26) Kim, S. J.; Smith, M. D.; Darriet, J.; zur Loye, H.-C. *J. Solid State Chem.* **2004**, *177*, 1493.

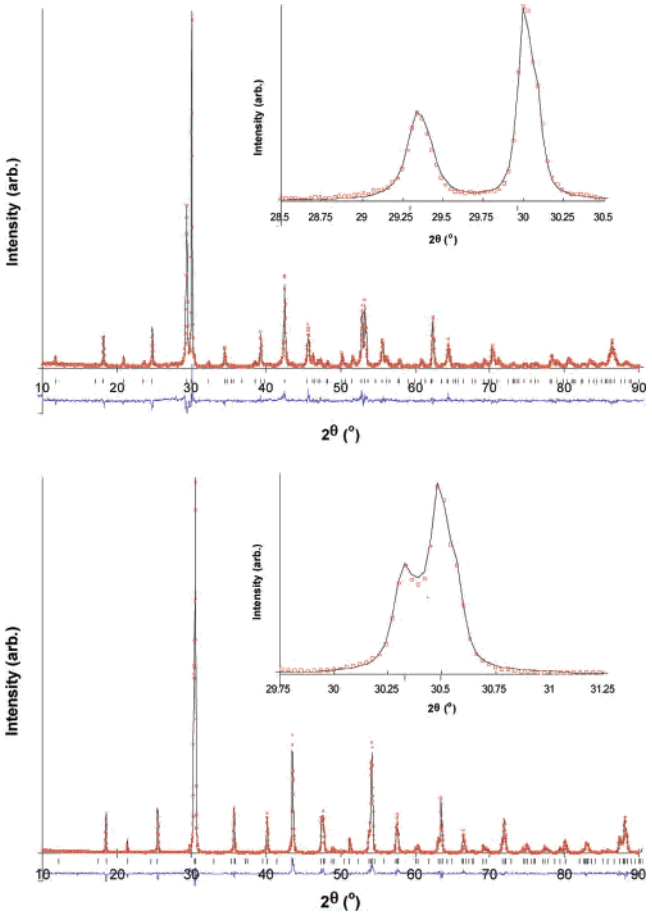


**Figure 1.** Ambient temperature X-ray powder diffraction data for $Ba_3LaRuIrO_9$ (top) and $Ba_3LuRuIrO_9$ (bottom). Circles are collected data, solid lines are fitted. Differences between observed and calculated intensities are shown below. Vertical marks indicate allowed peak positions. The inset shows the 104 and 110 reflections.

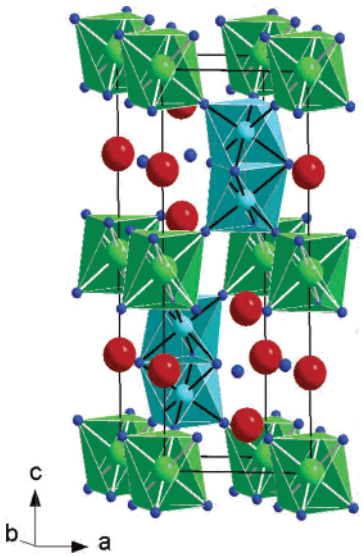


**Figure 2.** Crystal structure of $Ba_3LaRuIrO_9$ consisting of $(Ru/Ir)O_6$ face-sharing bioctahedra (cyan) corner-shared to $LaO_6$ octahedra (green). Barium cations are shown as red spheres and oxygen atoms as blue spheres.

did not result in an improvement to the fit. Magnetic susceptibility measurements, which are discussed in a subsequent section, also do not indicate any long-range magnetic ordering between Ru and Ir. Only a small difference is present between the ionic radii of $Ru^{4+}$ (0.62 Å) and $Ir^{4+}$ (0.625 Å) and between $Ru^{5+}$ (0.565 Å) and $Ir^{5+}$ (0.57 Å).[27] These data are consistent with the absence of long-range order in the cation arrangement of Ru and Ir in the face-sharing octahedra; typically, either a large size or a charge difference is needed to favor an ordered cation arrangement in this type of a structural situation, such as was observed in the low-temperature form of $Ba_3NaRu_2O_9$.[13]

Refined fractional coordinates obtained from the Rietveld refinements are given in Table 1. Additional information on the refined isotropic thermal parameters can be found in the Supporting Information. The variation within the lattice parameter as a function of the ionic radius of $Ln^{3+}$ is presented in Figure 3. The lattice parameter values all fall between those reported for $Ba_3LnIr_2O_9$ and $Ba_3LnRu_2O_9$.[3,4,7,8,18,28] The anomalously smaller lattice parameters of $Ba_3TbRuIrO_9$ and $Ba_3PrRuIrO_9$ are indicative of $Tb^{4+}$ and $Pr^{4+}$ rather than $Tb^{3+}$ and $Pr^{3+}$, respectively. These higher oxidation states effect an average oxidation state of only 4+ for the cations in the (Ir/Ru) dimer versus 4.5+ for all other compositions. The variation of the Ln−O(2) bond distances is shown in Figure 4a, where the short bond lengths of Pr−O(2) and Tb−O(2) are further indicative of the tetravalent oxidation state for those cations. These observations are in good agreement with the oxidation states reported for compounds in the $Ba_3LnIr_2O_9$ and $Ba_3LnRu_2O_9$ series.[3,7] Selected bond distances are given in Table 2, and additional bond distances and angles are given in the Supporting Information. The (Ru/Ir)−(Ru/Ir) bond distances range from 2.5 to 2.57 Å, which is typical for $Ba_3LnM_2O_9$ (M = Ru, Ir) perovskites.

A measure of the cation−cation repulsion is indicated in the center shift (Δ) of the (Ru/Ir) in the dimer. The center shift is defined as the distance between the (Ru/Ir) in the 4f Wyckoff position ($z \approx {}^1/_6$) and the ideal high-symmetry 4f cation position ($z = {}^1/_6$).[7] The center shift, shown in Figure 4b and illustrated in Figure 5, varies monotonically with a smaller shift for the larger rare earth cations. Positive center-shift values are indicative of cation−cation repulsion in the face-sharing dimer. The Δ values (0.024−0.073 Å) for $Ba_3Ln^{3+}IrRuO_9$ are slightly smaller than the values reported for $Ba_3Ln^{3+}Ir_2O_9$ (0.07−0.13 Å) and similar to the center shifts found in $Ba_3Ln^{3+}Ru_2O_9$ (0.027−0.073 Å).[7] It is worth noting that, while accurate center shifts can readily be extracted from the Rietveld refinements, an accurate determination of the (Ru/Ir)−O and Ln−O bond lengths from X-ray powder diffraction measurements is complicated. Although the quality of the data and refinements is high, the disordered mixture of Ru and Ir on a single crystallographic site and the difficulty in accurately locating the weakly scattering O near electron-dense cations such as Ba, Ir, and the lanthanides directs one to maintain a careful view in the analysis of the O positions and associated M−O bond lengths. To obtain very precise O positions, single-crystal X-ray or neutron powder diffraction experiments are preferred. The M−O bond distances obtained in this study are consistent with the

(27) Shannon, R. D. *Acta Crystallogr., Sect. A* **1976**, *32*, 751.
(28) Müller-Buschbaum, H.; Mertens, B. *Z. Anorg. Allg. Chem.* **1996**, *51*, 79.

**Table 1.** Isotropic Thermal Parameters and Background Subtracted $R_{wp}$ and $R_p$ Values[a]

| | $Ba_3YRuIrO_9$ | $Ba_3LaRuIrO_9$ | $Ba_3PrRuIrO_9$ | $Ba_3NdRuIrO_9$ | $Ba_3SmRuIrO_9$ |
|---|---|---|---|---|---|
| *a* (Å) | 5.8846(3) | 5.9588(8) | 5.8892(2) | 5.9375(3) | 5.9231(3) |
| *c* (Å) | 14.5494(9) | 15.093(2) | 14.6345(6) | 14.8177(8) | 14.7253(7) |
| vol (Å$^3$) | 436.33(4) | 464.11(12) | 439.56(3) | 452.40(4) | 447.39(4) |
| Ba2 *z* | 0.904 87(17) | 0.8952(2) | 0.902 30(14) | 0.899 95(16) | 0.902 29(15) |
| Ru/Ir *z* | 0.162 17(14) | 0.165 04(18) | 0.164 66(12) | 0.164 41(14) | 0.163 82(13) |
| O1 *x* | 0.5084(15) | 0.510(2) | 0.5154(16) | 0.5136(17) | 0.5146(17) |
| O2 *x* | 0.1648(15) | 0.1710(17) | 0.1721(14) | 0.1710(15) | 0.1733(14) |
| O2 *z* | 0.4142(8) | 0.4086(8) | 0.4152(7) | 0.4108(7) | 0.4118(7) |
| $R_{wp}$ (%) | 16.57 | 14.86 | 14.27 | 15.08 | 14.55 |
| $R_w$ (%) | 12.11 | 11.72 | 10.83 | 12.02 | 11.58 |
| $R(F^2)$ | 8.52 | 8.06 | 6.93 | 8.83 | 7.85 |
| $\chi^2$ | 3.31 | 2.91 | 2.27 | 2.61 | 2.47 |
| | $Ba_3EuRuIrO_9$ | $Ba_3GdRuIrO_9$ | $Ba_3TbRuIrO_9$ | $Ba_3DyRuIrO_9$ | $Ba_3HoRuIrO_9$ |
| *a* (Å) | 5.9169(3) | 5.9115(2) | 5.8452(3) | 5.8938(3) | 5.8866(2) |
| *c* (Å) | 14.6941(8) | 14.6600(6) | 14.4697(7) | 14.5841(7) | 14.5576(6) |
| vol (Å$^3$) | 445.51(4) | 443.67(3) | 428.14(3) | 438.74(3) | 436.87(3) |
| Ba2 *z* | 0.902 92(15) | 0.903 27(16) | 0.905 94(17) | 0.904 52(15) | 0.904 84(14) |
| Ru/Ir *z* | 0.163 59(13) | 0.163 45(15) | 0.162 49(14) | 0.162 61(13) | 0.162 28(12) |
| O1 *x* | 0.5164(17) | 0.5135(17) | 0.5087(18) | 0.5154(16) | 0.5129(15) |
| O2 *x* | 0.1691(14) | 0.1699(16) | 0.1657(17) | 0.1667(15) | 0.1668(13) |
| O2 *z* | 0.4125(7) | 0.4126(8) | 0.4135(8) | 0.4126(7) | 0.4132(7) |
| $R_{wp}$ (%) | 14.28 | 16.97 | 16.76 | 14.67 | 13.01 |
| $R_{wp}$ (%) | 11.48 | 13.40 | 13.55 | 11.71 | 10.32 |
| $R(F^2)$ | 7.71 | 9.90 | 9.50 | 8.27 | 7.96 |
| $\chi^2$ | 2.61 | 3.29 | 3.05 | 2.70 | 2.63 |

| | $Ba_3ErRuIrO_9$ | $Ba_3TmRuIrO_9$ | $Ba_3YbRuIrO_9$ | $Ba_3LuRuIrO_9$ |
|---|---|---|---|---|
| *a* (Å) | 5.8776(3) | 5.8728(2) | 5.8636(2) | 5.8580(3) |
| *c* (Å) | 14.5277(9) | 14.5041(6) | 14.4793(6) | 14.4644(7) |
| vol (Å$^3$) | 434.63(4) | 433.22(3) | 431.13(3) | 429.87(3) |
| Ba2 *z* | 0.905 17(15) | 0.905 56(12) | 0.906 38(14) | 0.906 68(14) |
| Ru/Ir *z* | 0.162 53(13) | 0.162 41(10) | 0.161 83(12) | 0.161 65(12) |
| O1 *x* | 0.5091(15) | 0.4903(12) | 0.5164(15) | 0.5101(14) |
| O2 *x* | 0.1688(15) | 0.1750(12) | 0.1682(13) | 0.1677(13) |
| O2 *z* | 0.4121(7) | 0.4136(7) | 0.4133(7) | 0.4122(7) |
| $R_{wp}$ (%) | 14.32 | 8.65 | 13.07 | 12.30 |
| $R_p$ (%) | 11.40 | 6.81 | 10.48 | 9.39 |
| $R(F^2)$ | 8.55 | 5.99 | 8.09 | 6.34 |
| $\chi^2$ | 2.80 | 1.86 | 2.54 | 2.38 |

[a] Atomic coordinates are Ba1(0, 0, $^1/_4$), Ba2($^1/_3$, $^2/_3$, *z*), M(0, 0, 0), Ru/Ir($^1/_3$, $^2/_3$, *z*), O1(*x*, 2*x*, $^1/_4$), and O2(*x*, 2*x*, *z*) in space group $P6_3/mmc$.

assigned oxidation states. The short (Ru/Ir)−(Ru/Ir) interatomic distances shown in Table 2 are similar to those observed for $Ba_3LnRu_2O_9$ and $Ba_3LnIr_2O_9$. The inner dimer (Ru/Ir)−O1−(Ru/Ir) bond angles given in Table 2 show very subtle changes throughout the series of compounds.

**3.b. Magnetic Susceptibility.** Short interatomic distances between the metal cations in the dimers have been shown to lead to strong magnetic interactions in the face-sharing octahedra.[10] The temperature dependence of the ZFC and FC magnetic susceptibilities are shown in Figures 6−9. Using the ZFC data, we calculated the effective magnetic moments at 2 and 300 K listed in Table 3 using eq 1

$$\mu_{eff} = \sqrt{3k_B\chi T/N_A} \quad (1)$$

where $k_B$ is the Boltzmann constant and $N_A$ is the Avogadro's number. Significantly smaller $\mu_{eff}$ values at 2 K compared to those at 300 K may be attributed to antiferromagnetic correlations, which reduce the magnetic moment.[7] Reduced magnetic moments in ruthenates and iridates have also been attributed to spin−orbit coupling.[20] Attempts to fit the susceptibility data with a standard Curie−Weiss law failed. A modified Curie−Weiss law, which includes a term for temperature-independent paramagnetism ($\chi_{tip}$), has been used previously in the analysis of the susceptibility data of triple perovskites.[7] The modified Curie−Weiss law is shown in eq 2

$$\chi = C/(T - \theta) + \chi_{tip} \quad (2)$$

The results of the fitting are shown as the solid curve in the inverse susceptibility. It should be noted that the values obtained from the susceptibility data are only approximate, since the susceptibilities are nonlinear in the temperature range of this study. Curie constants (*C*), Weiss constants ($\theta$), and $\chi_{tip}$ values obtained from the fitting of the magnetic susceptibility data are given in Table 3. The $\mu_{eff}$ (fit) was calculated from the fitted Curie constant. The $\chi_{tip}$ values obtained in the fitting procedure were on the order of $10^{-3}$ emu/mol. Although the magnitude of the $\chi_{tip}$ values are considerable, they are similar to the values that have been observed in previous magnetic studies of triple perovskites.[29]

In $Ba_3Ln^{3+}IrRuO_9$ compounds, there are two sensible combinations of oxidation states: (a) $Ir^{5+}/Ru^{4+}$ or (b) $Ir^{4+}Ru^{5+}$. Since the ionic sizes of $Ru^{4+}/Ir^{4+}$ and $Ru^{5+}/Ir^{5+}$

(29) Rijssenbeek, J. T.; Matl, P.; Batlogg, B.; Ong, N. P.; Cava, R. J. *Phys. Rev. B* **1998**, *58*, 10315.

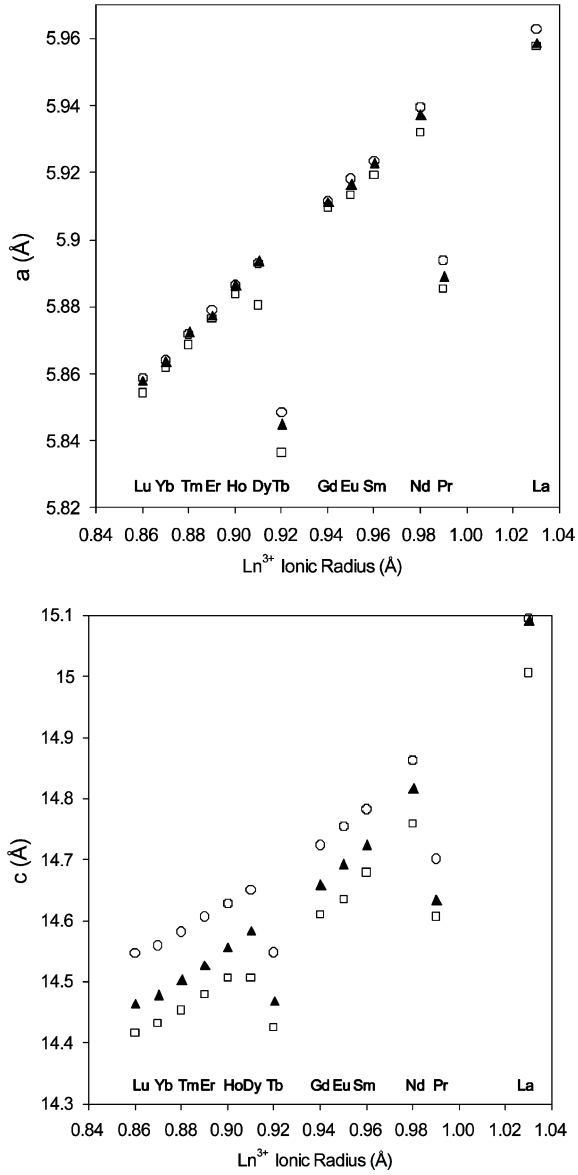


**Figure 3.** Lattice parameters versus $Ln^{3+}$ ionic radius. The standard uncertainty in the lattice parameter is smaller than the symbol size. Open circles represent $Ba_3LnIr_2O_9$, open squares $Ba_3LnRu_2O_9$, and filled triangles $Ba_3LnRuIrO_9$.

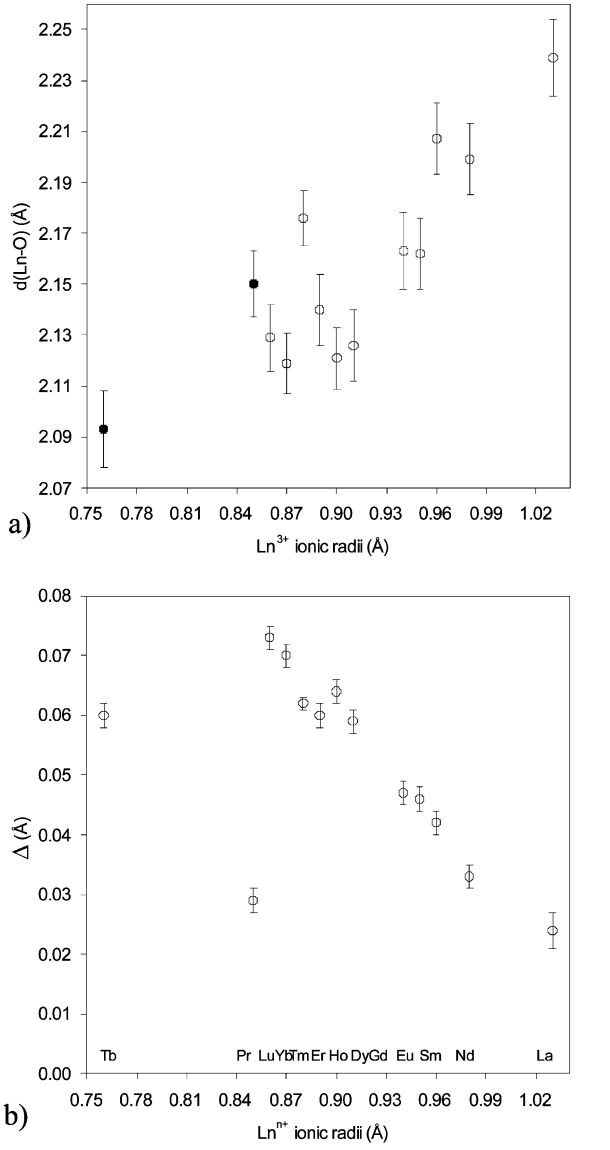


**Figure 4.** (a) Ln−O(2) bond distance versus ionic radii of $Ln^{n+}$ and (b) center shift, Δ, of Ru/Ir in the $[(Ru/Ir)O_6]$ dimer.

are very similar, it is not possible to distinguish the oxidation states using size considerations.[27] Consequently, an analysis of the magnetic susceptibility data was undertaken to distinguish between the possible combinations of formal oxidation states. The effective magnetic moment for each ion is needed in order to calculate the theoretical effective magnetic moment, which is calculated using eq 3.

$$\mu_{cal} = \sqrt{(\mu_{eff(Ln)})^2 + (\mu_{eff(Ru)})^2 + (\mu_{eff(Ir)})^2} \qquad (3)$$

The effective magnetic moments for Ir and Ru in their common oxidation states vary considerably. The effective magnetic moment for $Ir^{5+}$, with a singlet ground state, is nominally nonmagnetic at low temperatures, while an effective magnetic moment in the range 1.04−1.42 is observed near room temperature.[30−33] Ruthenium is known to adopt low spin states in perovskites and related structures; [10,34] thus, the spin-only effective magnetic moment for $Ru^{4+}$ ($d^4$) is 2.83 $\mu_B$. By comparison, the low-spin spin-only magnetic moment of $Ir^{4+}$ ($d^5$) has a $\mu_{eff} = 1.73\ \mu_B$. The expected effective magnetic moment for low-spin spin-only $Ru^{5+}$ ($d^3$) is 3.87 $\mu_B$; however, reduced magnetic moments are typically observed, for example, 1.5 $\mu_B$ in $Ba_3NiRu_2O_9$.[15] As shown in the crystal structure analysis, the octahedra are not rigorously octahedral but have three long and three short bonds. Although octahedral coordination is an approximation, a $t_{2g}$ and $e_g$ splitting was assumed for determining the number of unpaired electrons, and estimates of the theoretical

(30) Powell, A. V.; Gore, J. G.; Battle, P. D. *J. Alloys Compd.* **1993**, *201*, 73.
(31) Wakeshima, M.; Harada, D.; Hinatsu, Y. *J. Alloys Compd.* **1999**, *287*, 130.
(32) Hayashi, K.; Demazeau, G.; Pouchard, M.; Hagenmuller, P. *Mater. Res. Bull.* **1980**, *15*, 461.
(33) Battle, P. D.; Gore, J. G.; Hollyman, R. C.; Powell, A. V. *J. Alloys Compd.* **1995**, *218*, 110.
(34) Neumeier, J. J.; Hundley, M. F.; Smith, M. G.; Thompson, J. D.; Allgeier, C.; Xie, H.; Yelon, W.; Kim, J. S. *Phys. Rev. B* **1994**, *50*, 17910.

**Table 2.** Selected Interatomic Distances (Å)

| | $Ba_3YRuIrO_9$ | $Ba_3LaRuIrO_9$ | $Ba_3PrRuIrO_9$ | $Ba_3NdRuIrO_9$ | $Ba_3SmRuIrO_9$ |
|---|---|---|---|---|---|
| M−O2 (× 6) | 2.093(14) | 2.240(15) | 2.150(13) | 2.197(14) | 2.201(13) |
| (Ru/Ir)−O1 (× 3) | 2.194(12) | 2.232(18) | 2.237(14) | 2.237(14) | 2.251(15) |
| (Ru/Ir)−O2 (× 3) | 2.046(14) | 2.010(16) | 2.018(13) | 2.010(14) | 1.984(13) |
| (Ru/Ir)−(Ru/Ir) | 2.556(4) | 2.565(5) | 2.498(4) | 2.536(4) | 2.538(4) |
| (Ru/Ir)−O1−(Ru/Ir) (deg) | 71.2(4) | 70.1(5) | 67.9(4) | 68.8(4) | 68.4(4) |

| | $Ba_3EuRuIrO_9$ | $Ba_3GdRuIrO_9$ | $Ba_3TbRuIrO_9$ | $Ba_3DyRuIrO_9$ | $Ba_3HoRuIrO_9$ |
|---|---|---|---|---|---|
| M−O2 (× 6) | 2.158(13) | 2.160(15) | 2.093(15) | 2.126(14) | 2.118(12) |
| (Ru/Ir)−O1 (× 3) | 2.265(14) | 2.238(14) | 2.180(14) | 2.253(14) | 2.232(12) |
| (Ru/Ir)−O2 (× 3) | 2.020(13) | 2.011(15) | 2.022(15) | 2.024(14) | 2.023(12) |
| (Ru/Ir)−(Ru/Ir) | 2.540(4) | 2.538(4) | 2.532(4) | 2.549(4) | 2.554(3) |
| (Ru/Ir)−O1−(Ru/Ir) (deg) | 67.9(4) | 68.9(4) | 71.1(5) | 68.9(4) | 69.9(3) |

| | $Ba_3ErRuIrO_9$ | $Ba_3TmRuIrO_9$ | $Ba_3YbRuIrO_9$ | $Ba_3LuRuIrO_9$ |
|---|---|---|---|---|
| M−O2 (× 6) | 2.141(14) | 2.175(11) | 2.119(12) | 2.123(12) |
| (Ru/Ir)−O1 (× 3) | 2.194(12) | 2.041(9) | 2.255(13) | 2.202(11) |
| (Ru/Ir)−O2 (× 3) | 1.996(14) | 1.954(11) | 2.000(12) | 1.991(12) |
| (Ru/Ir)−(Ru/Ir) | 2.541(4) | 2.538(4) | 2.553(4) | 2.556(3) |
| (Ru/Ir)−O1−(Ru/Ir) (deg) | 71.0(3) | 77.0(3) | 68.8(3) | 70.8(3) |

effective magnetic moments of $Ba_3M^{3+}IrRuO_9$ were calculated using eq 3.

Two combinations of formal oxidation states were compared. The first a used a combination of noninteracting $M^{n+}$, with $\mu_{eff} = 0\ \mu_B$ for $Ir^{5+}$ at 2 K, $\mu_{eff} = 1.23\ \mu_B$ for $Ir^{5+}$ at 300 K,[32] and low-spin spin-only $Ru^{4+}$ with $\mu_{eff} = 2.83\ \mu_B$. The second combination used consisted of low-spin spin-only $Ir^{4+}$ ($\mu_{eff} = 1.73\ \mu_B$) and $Ru^{5+}$ with a reduced[15] effective magnetic moment ($\mu_{eff} = 1.5\ \mu_B$). Effective magnetic moments for $Ln^{3+}$ were taken from the literature.[5] The experimental $\mu_{eff}$ at 300 K calculated using eq 1 and the $\mu_{eff}$ obtained from the fitting of the susceptibility data with a temperature-independent paramagnetic term show slightly better agreement with the calculated theoretical effective magnetic moments assuming a $[Ir^{4+}Ru^{5+}O_9]$ dimer compared to a $[Ir^{5+}Ru^{4+}O_9]$ dimer. Using the assumption of a $[Ir^{5+}Ru^{4+}O_9]$ dimer, we found that the measured moments were, nonetheless, smaller than the predicted effective magnetic moments.

It is noteworthy that, in related double perovskites $Ba_2PrRuO_6$ and $Ba_2PrIrO_6$, it was found that $Ba_2PrRuO_6$ contains trivalent Pr and pentavalent Ru and that the iridium analogue, $Ba_2PrIrO_6$, is composed of tetravalent Pr and tetravalent Ir.[35,36] Consequently, a similar preference for Ru

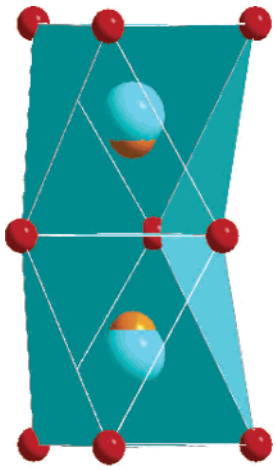

**Figure 5.** Illustration of the cation−cation repulsion and center shift in the [(RuIr)$O_9$] dimer. The blue sphere represents the actual (Ru/Ir) position, while the orange sphere represents the ideal high-symmetry position of (Ru/Ir).

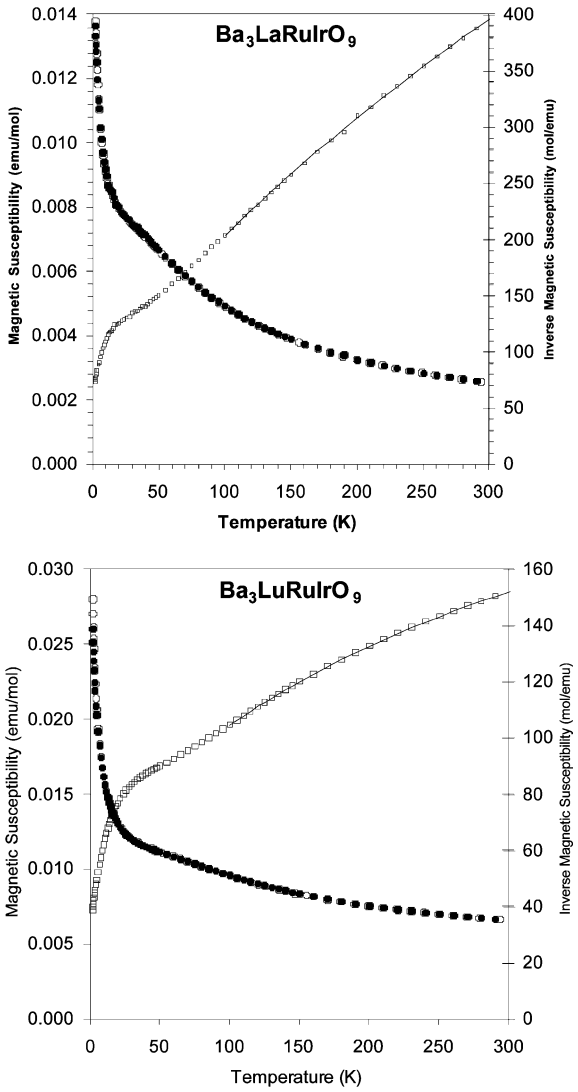


**Figure 6.** Temperature dependence of the zero-field-cooled (filled circle) and field-cooled (open circle) magnetic susceptibilities and (open square) inverse magnetic susceptibility at an applied field of 1 kG of (top) $Ba_3LaRuIrO_9$ and (bottom) $Ba_3LuRuIrO_9$.

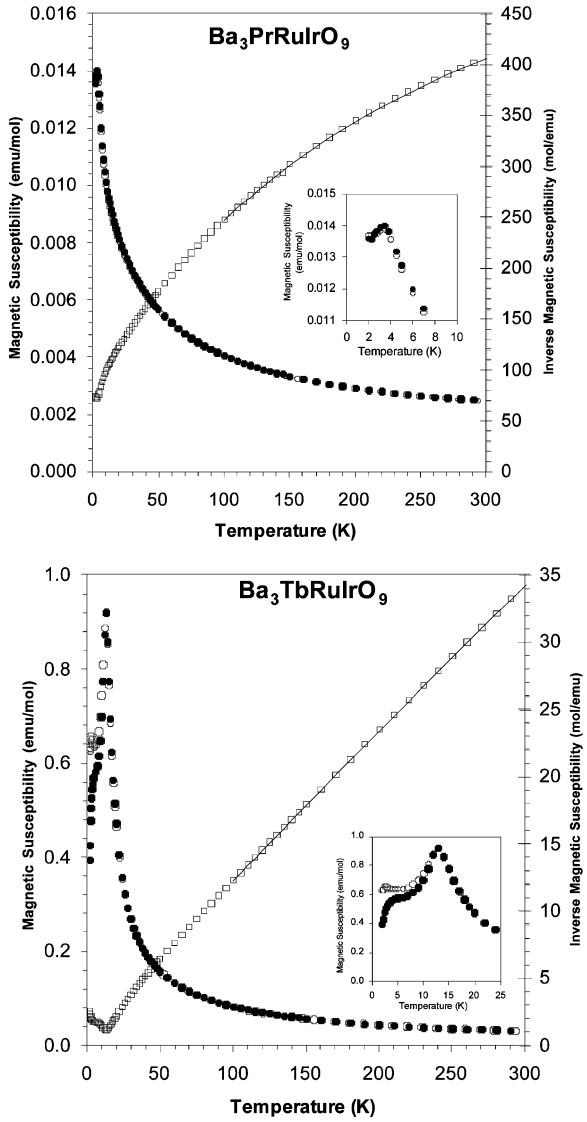


**Figure 7.** Temperature dependence of the zero-field-cooled (filled circle) and field-cooled (open circle) magnetic susceptibilities and (open square) inverse magnetic susceptibility at an applied field of 1 kG of (top) $Ba_3PrRuIrO_9$ and (bottom) $Ba_3TbRuIrO_9$.

to assume a higher formal oxidation state than Ir is reasonable in the triple perovskites of this study. Thus, the available information, the fit to the susceptibility data, the better agreement of the effective magnetic moments, and the oxidation state preference of ruthenium and iridium in related compounds strongly supports the assignment of the oxidation states of the magnetic cations as $Ru^{5+}$ and $Ir^{4+}$ in $Ba_3M^{3+}RuIrO_9$.

Nonetheless, even with the oxidation state assignment for ruthenium and iridium in these oxides, there remains the issue of their distribution in the dimers. To provide additional insight into the distribution of the cations in the dimer, the susceptibility data were examined in greater detail for compounds in which the M cation was magnetically inactive.

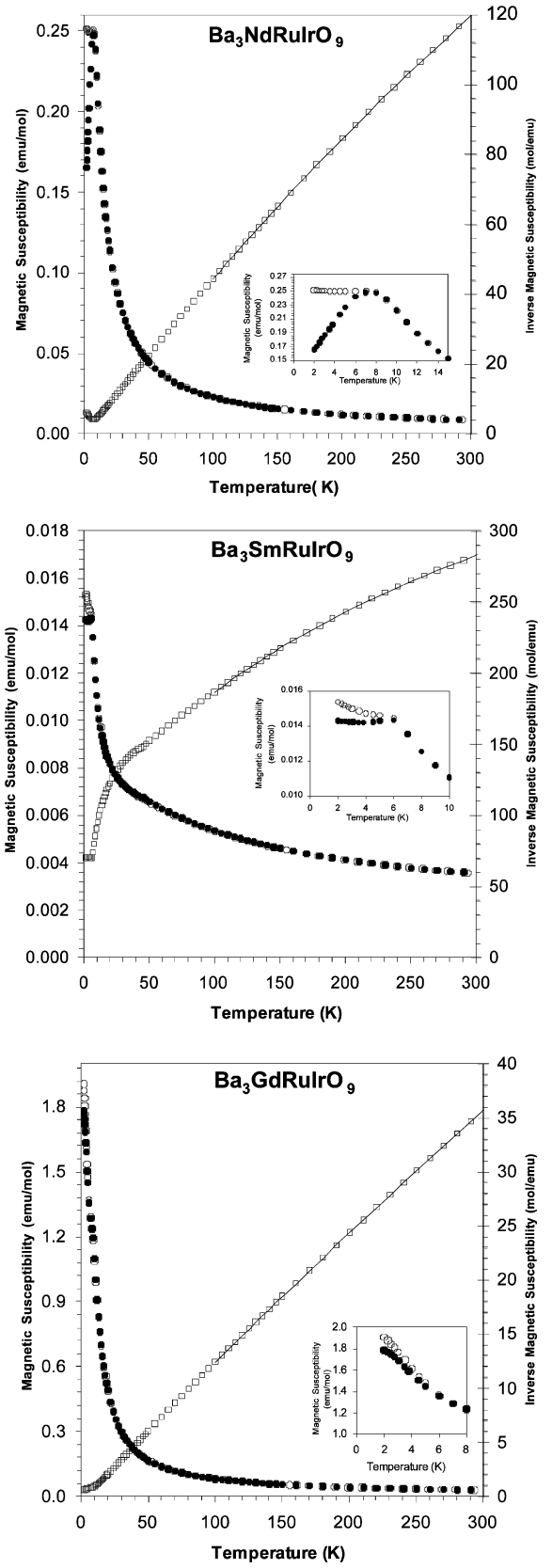


**Figure 8.** Temperature dependence of the zero-field-cooled (filled circle) and field-cooled (open circle) magnetic susceptibilities and (open square) inverse magnetic susceptibility at an applied field of 1 kG of (top) $Ba_3NdRuIrO_9$, (middle) $Ba_3SmRuIrO_9$, and (bottom) $Ba_3GdRuIrO_9$. The inset shows the divergence of the ZFC and FC data.

(35) Izumiyama, Y.; Doi, Y.; Wakeshima, M.; Hinatsu, Y.; Shimojo, Y.; Morii, Y. *J. Phys.: Condens. Matter* **2001**, *13*, 1303.
(36) Wakeshima, M.; Harada, D.; Hinatsu, Y. *J. Mater. Chem.* **2000**, *10*, 419.

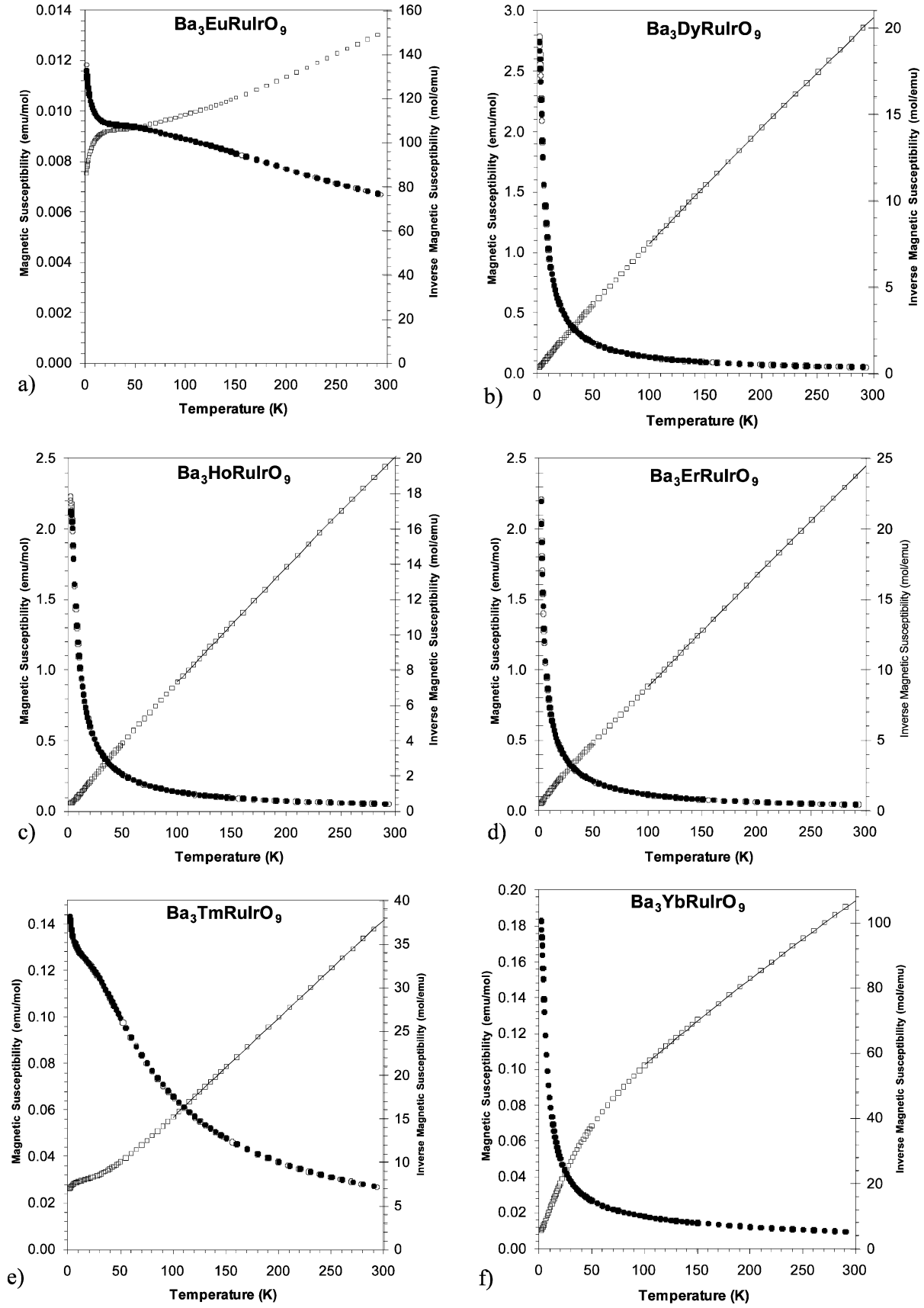


**Figure 9.** Temperature dependence of the zero-field-cooled (filled circle) and field-cooled (open circle) magnetic susceptibilities and (open square) inverse magnetic susceptibility at an applied field of 1 kG of (a) $Ba_3EuRuIrO_9$, (b) $Ba_3DyRuIrO_9$, (c) $Ba_3HoRuIrO_9$, (d) $Ba_3ErRuIrO_9$, (e) $Ba_3TmRuIrO_9$, and (f) $Ba_3YbRuIrO_9$.

**Table 3.** Magnetic Moment for Free $Ln^{3+}$ ($\mu_{Ln^{3+}}$), Calculated Magnetic Moments Using Each Magnetic Ion ($Ru^{5+}/Ir^{4+}$) ($\mu_{cal}$), Effective Magnetic Moments at 300 K ($\mu_{eff}$), Modified Curie−Weiss Fitting Results in the Temperature Range 100−300 K, and the Néel Temperature ($T_N$) or Temperature at Which the ZFC and FC Data Diverge ($T_{div}$)

| | $\mu_{eff}$ ($\mu_B$) (300 K) | $\mu_{eff}$ ($\mu_B$) (2 K) | $\mu_{eff}$ ($\mu_B$) (fit) | $\mu_{cal}$ ($\mu_B$) (300 K) | $C$ (emu/mol K) | $\chi_{tip}$ (emu/mol) | $\theta$ (K) | $T_N$ or $T_{div}$ |
|---|---|---|---|---|---|---|---|---|
| La | 2.46 | 0.47 | 2.27(3) | 3.08 | 0.65(2) | 0.000 69(4) | −54(3) | |
| Nd | 4.46 | 1.62 | 4.044(6) | 4.76 | 2.056(6) | 0.001 43(2) | 2.8(2) | 8 |
| Pr | 2.42 | 0.47 | 1.66(2) | | 0.345(8) | 0.001 42(2) | −31(2) | 4 |
| Sm | 2.91 | 0.48 | 2.18(2) | 3.45 | 0.599(9) | 0.001 94(2) | −75(2) | 6 |
| Eu | 3.98 | 0.43 | | 4.59 | | | | |
| Gd | 8.21 | 5.33 | 7.87(2) | 8.52 | 7.79(3) | 0.001 98(7) | 1.0(3) | 5 |
| Tb | 8.35 | 2.50 | 8.22(1) | | 8.49(2) | 0.001 48(5) | −5.6(2) | 13 |
| Dy | 10.77 | 6.61 | 10.52(1) | 11.07 | 13.92(2) | 0.003 26(8) | −7.0(2) | |
| Ho | 10.90 | 5.79 | 10.70(2) | 11.02 | 14.40(6) | 0.002 93(14) | −7.4(4) | |
| Er | 9.88 | 5.91 | 9.87(1) | 10.07 | 12.25(2) | 0.001 28(5) | −8.9(2) | |
| Tm | 7.95 | 1.51 | 8.23(2) | 8.16 | 8.51(4) | 0.000 74(8) | −30.5(5) | |
| Yb | 4.72 | 1.71 | 4.88(4) | 5.49 | 2.99(5) | 0.001 61(9) | −85(2) | |
| Lu | 2.25 | 0.34 | 2.87(2) | 3.08 | 1.039(10) | 0.003 86(2) | −81.7(13) | |
| Y | 2.73 | 0.40 | 2.23(2) | 3.08 | 0.624(10) | 0.001 60(2) | −115(2) | |

*3.b.i. $Ba_3MRuIrO_9$ (M = La, Lu, Y).* The compounds $Ba_3MRuIrO_9$ (M = La, Lu, Y) contain diamagnetic M cations, and consequently, the magnetic behavior of these compositions is due to the iridium and ruthenium cations in the face-sharing octahedral sites only. Magnetic susceptibility versus temperature data are shown in Figure 6 for M = La and Lu, and the Supporting Information contains data for M = Y. As might be expected, the data for these three compositions are qualitatively very similar. An upturn in the magnetic susceptibilities occurs as the temperature is decreased. The shape of the inverse magnetic susceptibility curve as a function of temperature may be modeled for these compounds by considering a dimer model that includes a distribution of metals and metal oxidation state combinations in the disordered (Ru/Ir) dimer. Three possible spin combinations in the dimer are a $S = {}^3/_2/S = {}^3/_2$ ($Ru^{5+}/Ru^{5+}$), $S = {}^1/_2/S = {}^1/_2$ ($Ir^{4+}/Ir^{4+}$), and $S = {}^3/_2/S = {}^1/_2$ ($Ir^{4+}/Ru^{5+}$). The $Ir^{+5}/Ru^{+4}$ case was not considered as it is thought unlikely that $Ru^{4+}$ would exist in the presence of $Ir^{5+}$. Fitting of the susceptibility data was carried out by considering a summation of three dimer scenarios following the description of exchange-coupled systems by Dillon and Darriet.[37] The general shape of the curve is reproduced; however, the magnetic behavior of the dimer is expected to approach zero at low temperatures in the inverse susceptibility versus temperature data. It was found that, for the compounds of this study, the curve approaches a more positive value at low temperatures and the model does not fit the data well below ∼15 K. The fit of the curve for $Ba_3LuRuIrO_9$ is shown in Figure 10 for 20 K < $T$ < 150 K. Resulting fit parameters are $g = 2.018(6)$, $J = -42.3(3)$ K, and $x = 0.3853(6)$, where $g$ is the gyromagnetic ratio, $J$ is the exchange interaction term, and $x$ is the dimer fraction term in $(1 - 2x)(Ir^{4+}/Ru^{5+}) + (x)(Ir^{4+}/Ir^{4+}) + (x)(Ru^{5+}/Ru^{5+})$. A constraint was utilized in that the number of $(Ru^{5+}/Ru^{5+})$ and $(Ir^{4+}/Ir^{4+})$ dimers were set equal to maintain consistency with the stoichiometry. If each of the two cations in the dimer were occupied completely randomly, then the expected value for $x$ is $x = 0.25$. If $x > 0.25$, then there is a tendency for the dimers to contain like cations, and if $x < 0.25$, then a mixed dimer with Ir/Ru occurs more often. In space group $P6_3/mmc$, the dimer cations occupy a single Wyckoff site where, hypothetically, it would be possible to have $x = 0$, meaning that all dimers contain exactly one iridium and one ruthenium but the two metals are disordered over the two positions of the dimer. The fitting results of the magnetic data indicate that there may be some short-range order with a slight preference for like-atom dimers; however, additional experiments such as pair distribution function analysis would be necessary to verify the presence of any short-range order in contrast to the long-range disorder found by X-ray diffraction analysis.

It is noteworthy that the gyromagnetic ratios, given in the Supporting Information, obtained from the fit of $Ba_3LaRuIrO_9$ and $Ba_3YRuIrO_9$ were smaller than the typical values of ∼2, and the values obtained from the fitting procedure should, therefore, be viewed with caution.

*3.b.ii. $Ba_3PrRuIrO_9$ and $Ba_3TbRuIrO_9$.* The susceptibility versus temperature data for $Ba_3PrRuIrO_9$, Figure 7, exhibit a downturn at approximately 3.5 K, consistent with antiferromagnetic correlations. These magnetic interactions may be due to magnetic ordering in the chemically disordered dimers, long-range order between the dimers, or an ordering of the

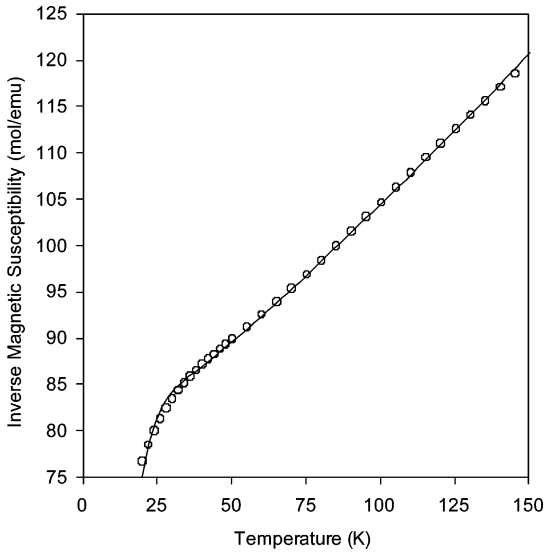


**Figure 10.** Inverse susceptibility versus temperature for $Ba_3LuRuIrO_9$. The line is the fit to the data using an exchange-coupled dimer model.

(37) Dillon, M.; Darriet, J. *Struct. Bonding* **1992**, *79*, 55.

$Pr^{4+}$ ions ($f^1$). Ordering of $Pr^{4+}$ in $Ba_3PrRu_2O_9$ or $Ba_3PrIr_2O_9$ was not observed.[3,7] Considering the lack of magnetic ordering of the $Pr^{4+}$ magnetic moments in isostructural $Ba_3PrRu_2O_9$ or $Ba_3PrIr_2O_9$, it seems unlikely that the transition at 3.5 K is related to the ordering of the $Pr^{4+}$ magnetic moments, but rather, it is caused by magnetic interactions of the dimers. The dimer may be composed of disordered $[Ru^{4+}Ir^{4+}O_9]$, which would have formal electron counts of $d^4$ and $d^5$. In case of antiferromagnetic coupling within the dimer, an ordering of the uncompensated spin ($S = {}^1/_2$) may occur between the dimers. Ordering of uncompensated magnetic moments in $[Ir^{4.5+}{}_2O_9]$ was suggested to occur for some compositions in $Ba_3LnIr_2O_9$ on the basis of specific heat anomalies.[5]

$Ba_3TbRuIrO_9$ undergoes a sudden decrease in the magnetic susceptibility at 13 K, as shown in Figure 7, consistent with antiferromagnetic correlations, and another change in the curvature of the susceptibility data at 2.5 K. It is noteworthy, in this regard, that the transition occurs at 13 K, a higher temperature than observed in the all-ruthenium analogue, $Ba_3TbRu_2O_9$. $Ba_3TbRu_2O_9$ was reported to undergo a magnetic phase transition at 9.5 K, in which the moments of $Tb^{4+}$ order antiferromagnetically along the *c* axis.[9] Interestingly, the all-iridium analogue, $Ba_3TbIr_2O_9$, did not exhibit any magnetic transition and had an effective magnetic moment of 8.10 $\mu_B$ and a Weiss constant of $-0.7$ K.[7] The transition at 13 K in $Ba_3TbRuIrO_9$ may, thus, be related to ordering of the $Tb^{4+}$ magnetic moments, and the second anomaly at 2K may be related to the ordering of the moments in the dimer in a manner similar to the behavior observed at 3.5 K in $Ba_3PrRuIrO_9$. Additional experiments are clearly warranted to investigate the transition temperature as a function of composition in the $Ba_3TbRu_{2-x}Ir_xO_9$ solid solution.

*3.b.iii. $Ba_3NdRuIrO_9$, $Ba_3SmRuIrO_9$, and $Ba_3GdRuIrO_9$.* $Ba_3NdRuIrO_9$, $Ba_3SmRuIrO_9$, and $Ba_3GdRuIrO_9$ exhibit a divergence between the ZFC and FC data, as shown in Figure 8. $Ba_3NdIr_2O_9$, by comparison, was reported to have a ferromagnetic transition at 17.4 K,[5] while $Ba_3NdRu_2O_9$ displayed a ferromagnetic transition at 24 K and a crystallographic phase transition at ca. 120 K.[4] The ferromagnetic ordering in each of these compounds was attributed to the ordering of the $Nd^{3+}$ magnetic moments. While $Ba_3NdRuIrO_9$ displays a divergence of the ZFC and FC data near 8 K, as shown in Figure 8, there is no evidence of long-range ferromagnetic order in this composition. The temperature dependence of the susceptibility suggests that the magnetic transition in $Ba_3NdRuIrO_9$ is of the antiferromagnetic type. The small positive Weiss temperature of 2.8(2) K may be an artifact of the fitting procedure. The Ru/Ir disorder in the dimers may prevent ferromagnetic coupling of the $Nd^{3+}$ moments in $Ba_3NdRuIrO_9$, in contrast to the ferromagnetic coupling observed in $Ba_3NdRu_2O_9$ and $Ba_3NdIr_2O_9$. This observation supports the coupling of the Nd moments through a pseudolinear next-nearest-neighbor Nd−O−(Ru/Ir)−O−Nd superexchange, rather than between nearest-neighbor Nd atoms, even in light of the fact that the distance of the first occurs over a longer distance (~8.4 Å) than the second (~5.9 Å). Although the crystal structures indicate the formation of solid solutions, the antiferromagnetic properties of $Ba_3NdRuIrO_9$ are in stark contrast to the ferromagnetic end members. Additional experiments are warranted to investigate the changeover in the magnetic properties in this solid-solution series.

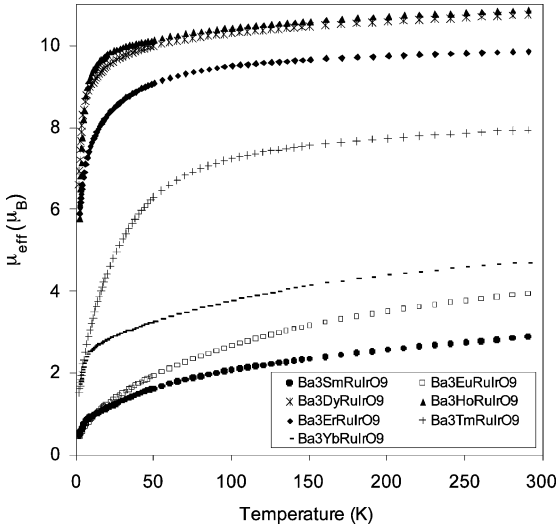


**Figure 11.** Effective magnetic moments versus temperature for $Ba_3LnRuIrO_9$ (Ln = Sm, Eu, Dy, Ho, Er, Tm, Yb).

$Ba_3SmRuIrO_9$ and $Ba_3GdRuIrO_9$ show a divergence near 6 K in the ZFC and FC data in Figure 9, consistent with antiferromagnetic interactions. In comparison, an antiferromagnetic transition was reported for $Ba_3GdIr_2O_9$ and an antiferromagnetic ordering of $Gd^{3+}$ was reported for $Ba_3GdRu_2O_9$.[7,18] The large negative Weiss constant, $-75(2)$ K, for $Ba_3SmRuIrO_9$ indicates antiferromagnetic interactions.

*3.b.iv. $Ba_3LnIrRuO_9$ (Ln = Eu, Dy, Ho, Er, Tm, Yb).* Magnetic susceptibilities of these compounds are shown in Figure 9 for Ln = Eu, Dy, Ho, Er, Tm, and Yb and exhibit similar behavior throughout the temperature range studied. The effective magnetic moments shown in Table 3, predicted using the spin-only contributions with a reduced moment for $Ru^{5+}$, are in good agreement with the effective magnetic moments obtained from fitting with a temperature-induced paramagnetic term. A decrease in the effective magnetic moments with temperature was observed in $Ba_3LnIrRuO_9$ (Ln = Eu, Dy, Ho, Er, Tm, Yb) and is shown in Figure 11. Similar behavior was observed in the magnetic susceptibilities of $Ba_3LnRu_2O_9$ (Ln = Eu, Dy, Ho, Er, Tm, Yb), which also showed a decrease in the effective magnetic moments with decreasing temperature.[8,38] The reduction in the effective magnetic moment is consistent with antiferromagnetic interactions, which tends to decrease the magnetic moments at low temperatures as the coupling becomes stronger. The negative Weiss constants shown in Table 3 also support the existence of antiferromagnetic correlations.

## Conclusions

The quinternary oxides $Ba_3MRuIrO_9$ (M = Y, lanthanides) adopt the 6H-$BaTiO_3$-type structure and crystallize in space

(38) Rath, M.; Müller-Buschbaum, H. *J. Alloys Compd.* **1994**, *210*, 119.

group $P6_3/mmc$. It was found that terbium and praseodymium in $Ba_3MRuIrO_9$ (M = Tb, Pr) were tetravalent, imparting an average oxidation state of 4+ for the Ru and Ir cations in the octahedral dimers. In the remaining compounds, all the rare earths were 3+, generating an average oxidation state of 4.5+ for the Ru and Ir cations in the octahedral dimers, which were assigned a formal oxidation state of $Ir^{4+}$ and $Ru^{5+}$. The bond distances between the disordered (Ir/Ru) in the face-sharing dimer ranged from 2.49 to 2.56 Å, consistent with the assigned oxidation states. A strong magnetic interaction between the cations in the face-sharing octahedra is observed in the magnetic susceptibility measurements. The measured effective magnetic moments were smaller than predicted from spin-only magnetic moments, indicative of spin−orbit coupling and strong exchange interactions within the disordered iridium/ruthenium octahedra pairs. In general, $Ba_3Ln^{3+}RuIrO_9$ compounds have negative Weiss constants and a decrease in the effective magnetic moments at low temperatures, consistent with antiferromagnetic correlations. Disorder in the dimer has an important influence on the magnetic properties, especially for the antiferromagnetic $Ba_3NdRuIrO_9$ that displays quite different properties than the ferromagnetic end members, which indicates that the magnetic coupling through the dimer has a significant impact on the observed properties.

**Acknowledgment.** Financial support from the Department of Energy through Grant DE-FG02-04ER46122 and the National Science Foundation through Grant DMR: 0450103 is gratefully acknowledged.

**Supporting Information Available:** Final annealing conditions for all compounds, additional information on the refined isotropic thermal parameters, additional bond distances and angles, magnetic susceptibility versus temperature data, and gyromagnetic ratios. This material is available free of charge via the Internet at http://pubs.acs.org.

IC051344Z